POSTTRANSLATIONAL MODIFICATIONS

Regulation of brain glutamate metabolism by nitric oxide and S-nitrosylation

Karthik Raju,[1] Paschalis-Thomas Doulias,[2] Perry Evans,[3] Elizabeth N. Krizman,[4] Joshua G. Jackson,[4] Oksana Horyn,[5] Yevgeny Daikhin,[5] Ilana Nissim,[5] Marc Yudkoff,[5] Itzhak Nissim,[5,6] Kim A. Sharp,[6] Michael B. Robinson,[1,4,7] Harry Ischiropoulos[1,2,7]*

Nitric oxide (NO) is a signaling intermediate during glutamatergic neurotransmission in the central nervous system (CNS). NO signaling is in part accomplished through cysteine S-nitrosylation, a posttranslational modification by which NO regulates protein function and signaling. In our investigation of the protein targets and functional impact of S-nitrosylation in the CNS under physiological conditions, we identified 269 *S*-nitrosocysteine residues in 136 proteins in the wild-type mouse brain. The number of sites was significantly reduced in the brains of mice lacking endothelial nitric oxide synthase ($eNOS^{-/-}$) or neuronal nitric oxide synthase ($nNOS^{-/-}$). In particular, $nNOS^{-/-}$ animals showed decreased S-nitrosylation of proteins that participate in the glutamate/glutamine cycle, a metabolic process by which synaptic glutamate is recycled or oxidized to provide energy. ^{15}N-glutamine–based metabolomic profiling and enzymatic activity assays indicated that brain extracts from $nNOS^{-/-}$ mice converted less glutamate to glutamine and oxidized more glutamate than those from mice of the other genotypes. GLT1 [also known as EAAT2 (excitatory amino acid transporter 2)], a glutamate transporter in astrocytes, was S-nitrosylated at Cys^{373} and Cys^{561} in wild-type and $eNOS^{-/-}$ mice, but not in $nNOS^{-/-}$ mice. A form of rat GLT1 that could not be S-nitrosylated at the equivalent sites had increased glutamate uptake compared to wild-type GLT1 in cells exposed to an S-nitrosylating agent. Thus, NO modulates glutamatergic neurotransmission through the selective, nNOS-dependent S-nitrosylation of proteins that govern glutamate transport and metabolism.

INTRODUCTION

Nitric oxide (NO) is an important physiological regulator of biological function in multiple tissues. NO-mediated signaling contributes to synaptic transmission and cerebrovascular coupling in the central nervous system (CNS) (*1*–*4*). The biological effects of NO are primarily achieved through two molecular mechanisms: (i) the activation of soluble guanylate cyclase and downstream guanosine 3′,5′-monophosphate (cGMP)–dependent signaling cascades, and (ii) S-nitrosylation, the posttranslational modification of reduced cysteine residues in proteins to generate *S*-nitrosocysteine. Protein S-nitrosylation has emerged as a vital mediator of protein function and signaling.

The neuronal isoform of nitric oxide synthase (nNOS) produces NO in the brain. Mice with a genetic deletion of nNOS ($nNOS^{-/-}$) demonstrate various phenotypic insufficiencies (*5*), including deficits in several forms of memory (*6*–*9*). Furthermore, these mice have decreased presynaptic/postsynaptic excitability (*10*, *11*) and synaptic plasticity (*12*–*14*), effects that may be due to impaired glutamatergic neurotransmission. Additionally, $nNOS^{-/-}$ mice exhibit reduced neurodegeneration after cerebral ischemia, which may be because of reduced glutamate excitotoxicity (*15*, *16*). Therefore, nNOS-derived NO could affect synaptic activity by regulating glutamate availability. Many of the effects of NO on neurotransmission occur independently of cGMP activation (*17*–*19*), suggesting another mechanism for NO-dependent regulation of neurotransmission.

Protein S-nitrosylation is an alternative biochemical and molecular pathway by which NO could influence neurotransmission in the CNS (*20*). Selective protein S-nitrosylation has been linked to a few postsynaptic processes, including the regulation of NMDA (*N*-methyl-D-aspartate) receptor and AMPA receptor activity, synaptic targeting of PSD-95, gephyrin clustering at GABAergic [GABA (γ-aminobutyric acid)–releasing] synapses, surface expression of AMPA receptors, and D-serine production (*21*–*27*). However, the biological functions of protein S-nitrosylation in the tripartite glutamatergic synapse remain mostly unknown. Here, we used mass spectrometry (MS)–based proteomic methodologies to identify protein *S*-nitrosocysteine residues in brain homogenates from wild-type, $nNOS^{-/-}$, and $eNOS^{-/-}$ (lacking endothelial nitric oxide synthase) mice. When coupled with metabolomic profiling, enzyme activity measurements, and site-directed mutagenesis, the proteomic data indicate that reversible protein S-nitrosylation regulates glutamate uptake, metabolism, conversion to glutamine, and glutamatergic transmission.

RESULTS

Ontological analysis of brain S-nitrosylated proteins

Mass spectrometric analysis of endogenous S-nitrosylated proteins using organomercury-based enrichment approaches (*28*–*30*) unearthed 269 sites in 136 proteins in wild-type mouse brain, 135 sites in 95 proteins in $eNOS^{-/-}$ brain, and 71 sites in 53 proteins in $nNOS^{-/-}$ brain (Fig. 1A and table S1). The reduction in the S-nitrosylation of residues and proteins in $nNOS^{-/-}$ (74%) and $eNOS^{-/-}$ mice (50%) implied that both NOS isoforms contributed substantially to endogenous protein S-nitrosylation (fig. S1). To place these observations in biological context, we performed gene ontology (GO) analysis. First, we constructed a reference mouse brain proteome consisting of 7025

[1]Neuroscience Graduate Group, University of Pennsylvania, Philadelphia, PA 19104, USA. [2]Division of Neonatology, Department of Pediatrics, Children's Hospital of Philadelphia Research Institute, Philadelphia, PA 19104, USA. [3]Department of Biomedical and Health Informatics, Children's Hospital of Philadelphia Research Institute, Philadelphia, PA 19104, USA. [4]Division of Neurology, Department of Pediatrics, Children's Hospital of Philadelphia Research Institute, Philadelphia, PA 19104, USA. [5]Division of Genetic and Metabolic Disease, Department of Pediatrics, Children's Hospital of Philadelphia Research Institute, Philadelphia, PA 19104, USA. [6]Department of Biochemistry and Biophysics, University of Pennsylvania, Philadelphia, PA 19104, USA. [7]Department of Systems Pharmacology and Translational Therapeutics, University of Pennsylvania, Philadelphia, PA 19104, USA.
*Corresponding author. E-mail: ischirop@mail.med.upenn.edu

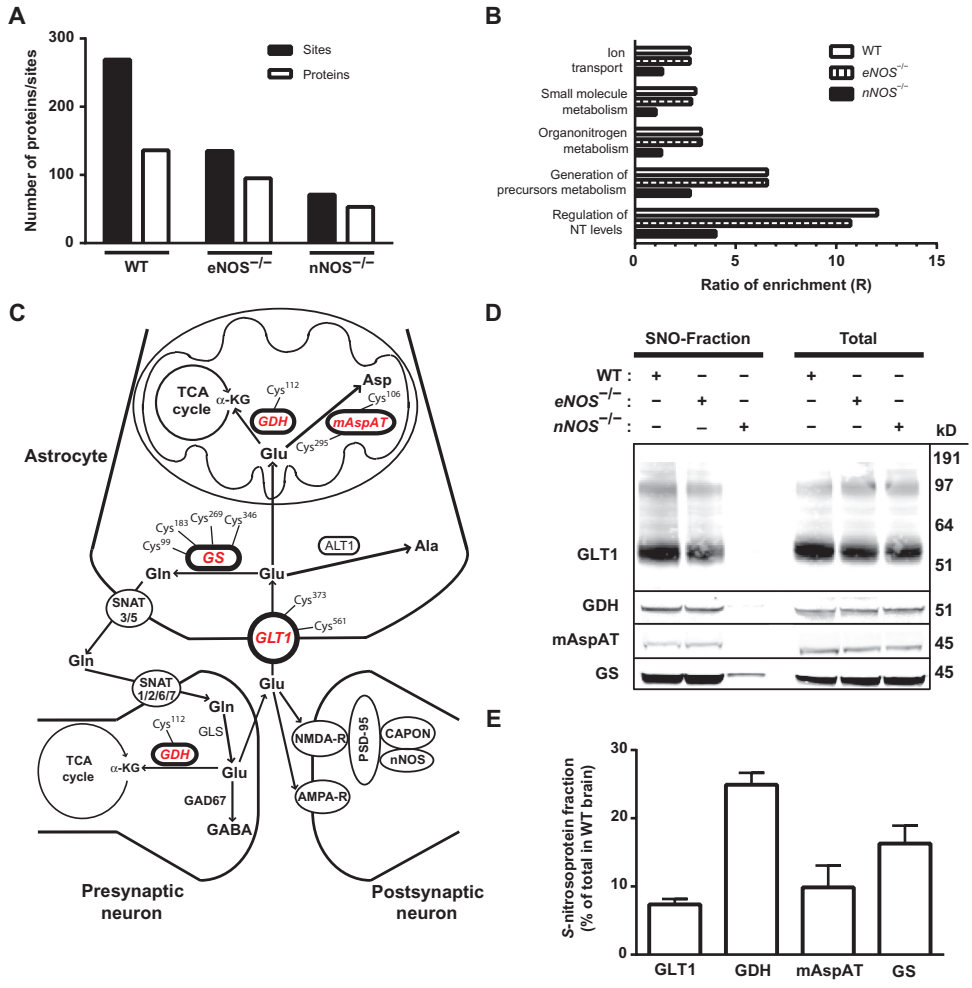

Fig. 1. Proteomic identification of protein *S*-nitrosocysteine residues and GO analysis of modified proteins in wild-type (WT), *eNOS*$^{-/-}$, and *nNOS*$^{-/-}$ mouse brain. (**A**) Identification of S-nitrosylated proteins and their corresponding sites of modification in mouse brain (n = 6 mice per genotype). (**B**) GO-based functional clustering of S-nitrosylated proteins in each genotype. The ratio of enrichment (R) score is calculated as the ratio of the observed number (O) of S-nitrosylated proteins with a specific GO annotation in the WebGestalt database to the number of annotated proteins expected (E) to be in the *S*-nitrosocysteine proteome. Only the top five pathways in the WT mouse with the lowest P values were considered ($P < 0.01$). NT, neurotransmitter. (**C**) Schematic of glutamate metabolism. Proteins are denoted by their short protein names, as assigned by UniProt: GLT1 (excitatory amino acid transporter 2), GDH (glutamate dehydrogenase), mAspAT (mitochondrial aspartate aminotransferase), and GS (glutamine synthetase). S-nitrosylated proteins are italicized, with the associated sites of modification indicated. Gln, glutamine; Glu, Glutamate; Asp, aspartate; Ala, alanine; α-KG, α-ketoglutarate; Cys, cysteine. (**D**) NOS-based dependence of S-nitrosylation (SNO) of glutamate/glutamine cycle effectors. Modified proteins (denoted as the "SNO-Fraction") within the aforementioned pathway were confirmed by Western blot against specific targets in all genotypes. The total abundance of the indicated protein targets in 30 μg of total homogenate did not obviously differ between genotypes (n = 2 mice per genotype). (**E**) Quantification of the relative S-nitrosylated fraction for each glutamate/glutamine cycle protein in WT mouse brain. Bars represent means ± SEM (n = 3 mice).

proteins curated from previously published reports (*31*–*34*) and our experimental data. Using this reference proteome as a background, we performed computational analysis using WebGestalt (*35*) and identified several molecular pathways and cellular processes in which S-nitrosylated proteins were significantly enriched in the wild-type brain (Fig. 1B and fig. S2). The computed ratio of enrichment for the top five pathways was similar between wild-type and *eNOS*$^{-/-}$ brains but was reduced in *nNOS*$^{-/-}$ brains (Fig. 1B). For example, the molecular processes associated with the regulation of neurotransmitter levels showed a 67% reduction in *nNOS*$^{-/-}$ brains, a finding consistent with previous descriptions of synaptic deficits in the *nNOS*$^{-/-}$ mice (*6*–*14*). Within the regulation of neurotransmitter level pathway, we mapped *S*-nitrosocysteine residues in four proteins: excitatory amino acid transporter 2, glutamate dehydrogenase, mitochondrial aspartate aminotransferase, and glutamine synthetase (Fig. 1C). The first three proteins were S-nitrosylated in wild-type and *eNOS*$^{-/-}$ mice, but not in *nNOS*$^{-/-}$ mice, whereas glutamine synthetase showed reduced S-nitrosylation in *nNOS*$^{-/-}$ mice as compared to wild-type and *eNOS*$^{-/-}$ mice (Fig. 1D and table S1). We confirmed the mass spectrometric–based identification of these S-nitrosylated proteins by Western blotting (Fig. 1D) and quantified the fraction of each protein modified by S-nitrosylation in wild-type brain (Fig. 1E). These four proteins are major contributors in the glutamate/glutamine cycle (*36*–*39*), the biological process responsible for managing the metabolic fate and availability of glutamate in the synapse. Overall, the proteomic and ontological analysis indicates that proteins involved in the glutamate/glutamine cycle are selectively S-nitrosylated by nNOS, implying a role for NO in the regulation of glutamate metabolism.

Regulation of glutamate/glutamine metabolism by NO

To study the effects of nNOS-derived NO and protein S-nitrosylation on the glutamate/glutamine cycle, we quantified the fractional isotopic enrichment of glutamate-associated metabolites in acutely isolated hippocampal slices after treatment with [2-^{15}N] L-glutamine (fig. S3). Steady-state amounts of labeled glutamate-associated metabolites were quantified by high-performance liquid chromatography (HPLC) and gas chromatography–mass spectrometry (GC-MS) approaches (*40*, *41*) under stimulatory (Mg^{2+}-free) conditions in wild-type, *eNOS*$^{-/-}$, and *nNOS*$^{-/-}$ mice. The three genotypes showed similar total amounts of glutamate, glutamine, aspartate, alanine, and GABA (Fig. 2A), indicating a lack of gross metabolic dysfunction. However, the ratio of intracellular glutamine to glutamate was 30% higher in *nNOS*$^{-/-}$ mice, reflecting potential perturbations in glutamate handling (Fig. 2B). ^{15}N-fractional isotopic

enrichment for alanine, aspartate, and glutamate ranging between 20 and 30% was significantly decreased in *nNOS*$^{-/-}$ brain slices relative to the other two genotypes, confirming altered glutamate allocation in *nNOS*$^{-/-}$ mice (Fig. 2C).

To further explore the influence of nNOS-derived NO on the glutamate/glutamine cycle, we performed enzymatic assays for glutamate dehydrogenase, mitochondrial aspartate aminotransferase, and glutamine synthetase in mitochondrial extracts and brain homogenates (Fig. 2D). The activities of glutamate dehydrogenase and mitochondrial aspartate aminotransferase were significantly increased in *nNOS*$^{-/-}$ mitochondrial extracts as compared to wild-type and *eNOS*$^{-/-}$ mice (Fig. 2D). Trans-illumination of wild-type mitochondrial extracts with ultraviolet (UV) light, a treatment that effectively eliminates NO from *S*-nitrosocysteine residues (*42*, *43*), increased the enzymatic activities of glutamate dehydrogenase and mitochondrial aspartate aminotransferase in wild-type extracts similar to that measured in *nNOS*$^{-/-}$ extracts (Fig. 2D). We used selective inhibitors guanosine 5′-triphosphate (GTP) (for glutamate dehydrogenase) and aminooxyacetic acid (AOAA) (for mitochondrial aspartate aminotransferase) to validate the specificity of the assays. Each inhibitor resulted in >95% loss of activity (Fig. 2D). Relative to wild-type homogenate, glutamine synthetase activity was decreased slightly in *nNOS*$^{-/-}$ but not in *eNOS*$^{-/-}$ brain homogenate (Fig. 2D). UV trans-illumination decreased the activity of glutamine synthetase in wild-type homogenate (Fig. 2D). The difference in the reduction in glutamine synthetase activity between *nNOS*$^{-/-}$ mice and wild-type mice exposed to UV light most likely reflects contributions from additional NOS isoforms to the S-nitrosylation of glutamine synthetase in vivo (Fig. 1D and table S1). Exposing wild-type homogenate to the glutamine synthetase inhibitor L-methionine sulfoximine (MSO) (*44*) resulted in a >95% loss of activity (Fig. 2D). Together, metabolomic profiling and enzymatic activity assays imply that selective nNOS-dependent S-nitrosylation of key proteins in the glutamate/glutamine cycle regulates glutamate metabolism.

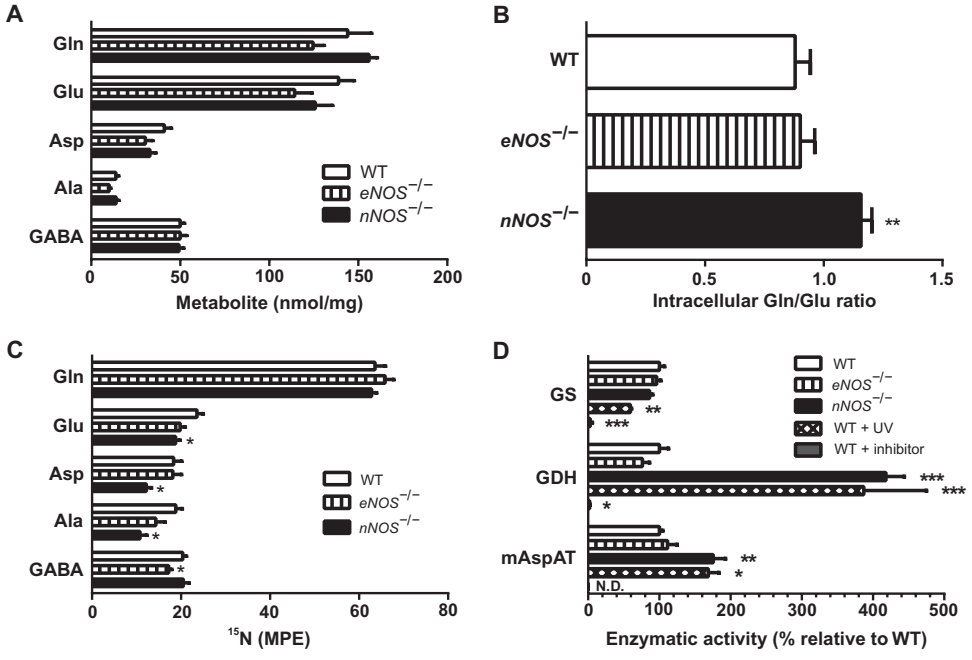

Fig. 2. Analysis of the glutamate/glutamine cycle in WT, *eNOS*$^{-/-}$, and *nNOS*$^{-/-}$ mouse brain. (A) Glutamate-associated metabolite quantification. Total metabolite concentrations were determined by HPLC and normalized to protein content ($n = 3$ mice per genotype). (B) Intracellular glutamine/glutamate ratios. $^{**}P < 0.01$ as determined by one-way analysis of variance (ANOVA) with Tukey post hoc analysis ($n = 3$ mice per genotype). (C) Genotypic differences in steady-state glutamine/glutamate metabolism. ^{15}N enrichment of glutamine/glutamate and associated metabolites was determined using GC-MS as in (*41*), and presented as ^{15}N molar percent excess (MPE) of M+1 isotopomer. $^{*}P < 0.05$ compared to WT by one-way ANOVA with Tukey post hoc analysis between genotypes ($n = 3$ mice per genotype). (D) Enzymatic activity of glutamate/glutamine effectors. Bars represent mean ± SEM ($n = 3$ mice per genotype) and indicate enzymatic activity relative to that measured in untreated extracts from WT mice. Activities in untreated WT extracts: GS = 1259 ± 94 nmol/mg per hour, GDH = 120 ± 15 nmol/mg per minute, mAspAT = 238 ± 12 nmol/mg per minute. WT + UV denotes extracts exposed to UV trans-illumination before assessing enzymatic activity. WT + inhibitor denotes extracts pretreated with specific enzymatic inhibitors (GS = 0.5 mM MSO, GDH = 20 μM GTP, mAspAT = 1 mM AOAA). N.D., not detectable. $^{*}P < 0.05$, $^{**}P < 0.01$, $^{***}P < 0.001$ as compared to WT by one-way ANOVA with Tukey post hoc analysis.

Regulation of intracellular transport of glutamate by the S-nitrosylation of excitatory amino acid transporter 2

Excitatory amino acid transporter 2 (also known as glutamate type I transporter) is the primary transporter responsible for glutamate uptake in astrocytes of the cerebral cortex (*45*). Genetic deletion of the transporter results in lethal epileptic seizures in mice and eventually leads to limited postnatal viability (*46*, *47*). Because of its importance in physiological synaptic function (*48*), as well as its identification in the brain *S*-nitrosocysteine proteome, we explored the functional consequences of the *S*-nitrosylation of excitatory amino acid transporter 2 in mouse brain synaptosomal preparations, as well as in a cell model. We quantified sodium (Na^+)–dependent glutamate uptake in freshly prepared synaptosomes from wild-type, *nNOS*$^{-/-}$, and *eNOS*$^{-/-}$ forebrain in the presence or the absence of dihydrokainate (DHK), which inhibits excitatory amino acid transporter 2 (*49*). The resulting difference in uptake activity between the two treatments (DHK-sensitive) is the glutamate uptake mediated by excitatory amino acid transporter 2. Synaptosomal DHK-sensitive glutamate uptake was increased in *nNOS*$^{-/-}$ synaptosomes as compared to wild-type synaptosomes (Fig. 3A). Elimination of NO from *S*-nitrosocysteine residues by pretreatment of wild-type synaptosomes with copper plus ascorbate (*50*) increased DHK-sensitive glutamate uptake, indicating a functional regulatory role for S-nitrosylation. On the other hand, DHK-insensitive Na^+-dependent glutamate was similar in synaptosomes prepared from the three genotypes, or in synaptosomes prepared from wild-type mice after treatment with copper and ascorbate, suggesting that excitatory amino acid transporter 2–independent uptake was unaffected by the altered concentrations of NO or the elimination of S-nitrosylation (fig. S4A). We further explored the functional effect of S-nitrosylation in human embryonic kidney (HEK)–293T cells that were transiently transfected with plasmids expressing either the wild-type rat transporter or a double point mutant (C373S/C562S) of the two in vivo

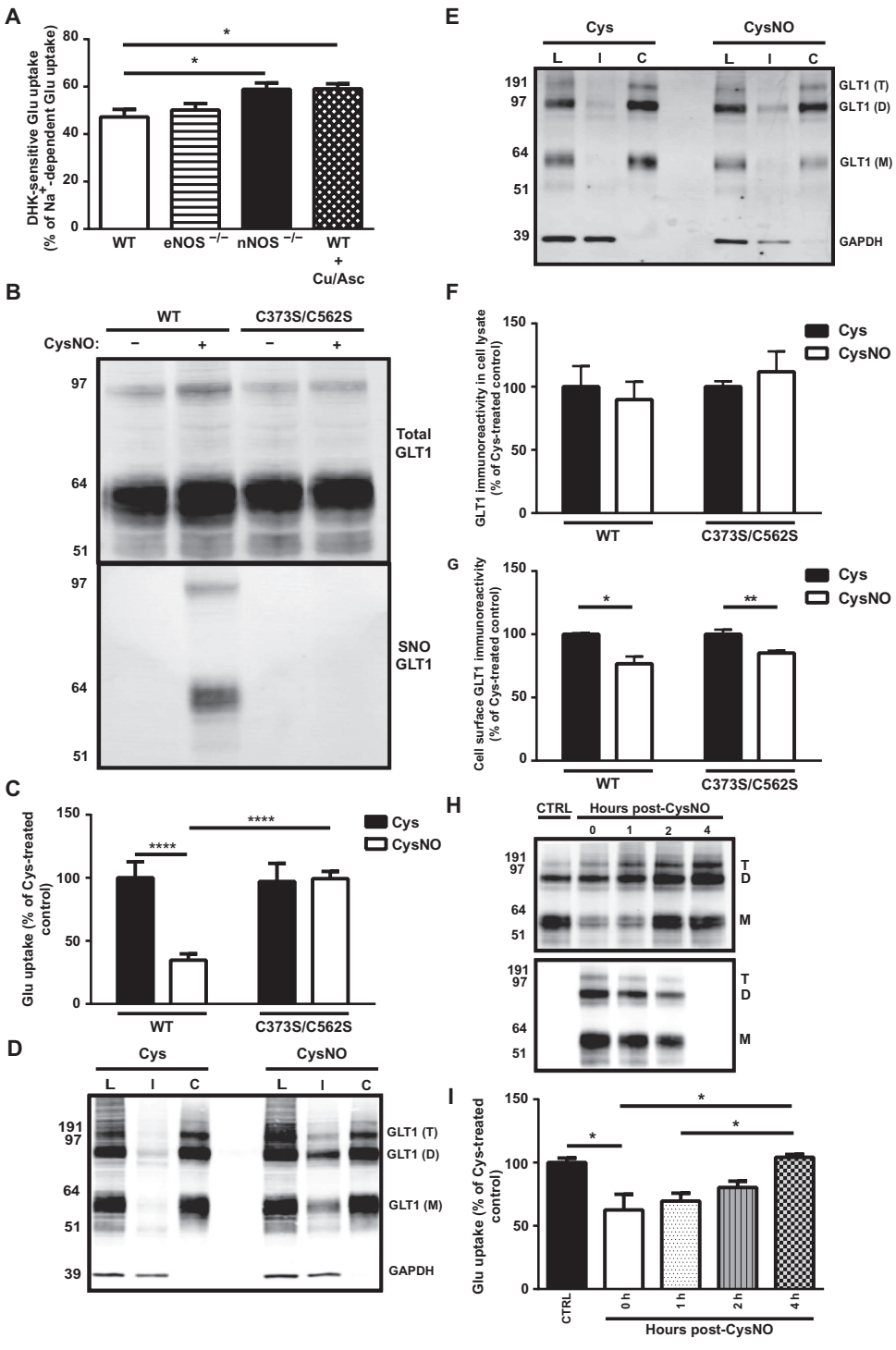

Fig. 3. Regulation of GLT1 function by S-nitrosylation. (A to I) All results are summarized from three mice per genotype (A) or three independent experiments in cells (B to I), and plotted as means ± SEM. Cells were treated with L-cysteine (Cys) or *S*-nitrosocysteine (CysNO). (A) The fraction of total Na^+-dependent glutamate uptake that was DHK-sensitive was greater in synaptosomes from $nNOS^{-/-}$ mice or synaptosomes pretreated with copper and ascorbate (WT + Cu/Asc) than in untreated WT synaptosomes. Na^+-dependent uptake in untreated synaptosomes of the indicated genotype: WT = 0.24 ± 0.03 nmol/mg per minute, $nNOS^{-/-}$ = 0.26 ± 0.06 nmol/mg per minute, $eNOS^{-/-}$ = 0.25 ± 0.04 nmol/mg per minute, and WT + Cu/Asc = 0.29 ± 0.03 nmol/mg per minute. **P* < 0.05 after one-way ANOVA followed by Dunnett's post hoc analysis. (B and C) S-nitrosylation of WT GLT1 in HEK-293T cells after CysNO treatment (B) correlated with decreased glutamate uptake (C). Cys-treated WT GLT1 = 0.27 ± 0.03 nmol/mg per minute, Cys-treated C373S/C562S GLT1 = 0.26 ± 0.04 nmol/mg per minute. *****P* < 0.0001 after two-way ANOVA followed by Bonferroni post hoc analysis. (D and E) Representative blots from cell surface biotinylation assays of cells expressing WT GLT1 (D) and C373S/C562S GLT1 (E). L, lysate; I, intracellular fraction; C, cell surface fraction. Five micrograms of total lysate and equivalent dilutions of the other fractions were used. T, D, and M refer to trimeric, dimeric, and monomeric GLT1, respectively. The intracellular fraction of both forms of GLT1 was increased after CysNO treatment. (F) Quantification of total GLT1 abundance in cell lysate. (G) Quantification of plasma membrane abundance of GLT1 after Cys/CysNO treatment. **P* < 0.05, ***P* < 0.01 as determined by ANOVA with Bonferroni post hoc analysis. (H and I) S-nitrosylation of WT GLT1 was reversible (H) and correlated with a recovery in glutamate uptake (I). WT GLT1 cells were exposed to Cys (CTRL) or CysNO, then to fresh medium. Glutamate uptake and S-nitrosylation of GLT1 were assessed after CysNO exposure. **P* < 0.05 after one-way ANOVA followed by Bonferroni post hoc analysis. GAPDH, glyceraldehyde-3-phosphate dehydrogenase.

S-nitrosylated cysteine residues. The cysteine residue at position 562 in the rat sequence corresponds to cysteine 561 in the mouse sequence because the rat homolog of excitatory amino acid transporter 2 is one amino acid longer than the mouse protein. To induce protein S-nitrosylation, we treated cells with a nonphysiological concentration of *S*-nitrosocysteine, which is taken up through the L-amino acid transport system. *S*-nitrosocysteine is an *S*-nitrosylating agent that can transfer an NO equivalent to reduced cysteine residues in proteins (*51*). As a control, cells were treated with the same concentration of cysteine. Treatment of cells with *S*-nitrosocysteine resulted in S-nitrosylation of the wild-type transporter (Fig. 3B), which correlated with decreased glutamate uptake (Fig. 3C). The C373S/C562S transporter was not S-nitrosylated in *S*-nitrosocysteine–treated cells (Fig. 3B), and its

activity was similar to that of wild-type transporter and was unaffected by *S*-nitrosocysteine treatment (Fig. 3C). Mutation of one cysteine residue (either 373 or 562) to serine resulted in transporter activity sensitive to *S*-nitrosocysteine treatment, indicating that the modification of either cysteine residues is sufficient for S-nitrosylation–mediated inhibition of glutamate transport (fig. S4B). Relative to L-cysteine treatment, exposure of cells to *S*-nitrosocysteine did not alter the protein abundance of the wild-type or the C373S/C562S mutant transporter (Fig. 3, D to F), but decreased the surface abundance of both transporters by 20 to 25% (Fig. 3G). Kinetic analysis of glutamate uptake mediated by excitatory amino acid transporter 2 (fig. S4C) revealed an 81% decrease in the K_m (Michaelis constant) of the wild-type transporter after *S*-nitrosocysteine treatment and an 84% decrease in V_{max}. Removal of *S*-nitrosocysteine from the medium led to a gradual decrease in the S-nitrosylation of wild-type transporter that correlated with a recovery in glutamate uptake activity (Fig. 3, H and I). Overall, these data suggest that specific and reversible S-nitrosylation of excitatory amino acid transporter 2 at Cys^{373} and Cys^{562} regulates the activity of the transporter.

Molecular modeling of the effects of S-nitrosylation

We used the crystal structure of mouse mitochondrial aspartate aminotransferase [Protein Data Bank (PDB) 3PD6], human glutamate dehydrogenase (PDB 1L1F), and human glutamine synthetase (PDB 2QC8) as templates and generated protein structures with the specific S-nitrosylated cysteine residues. Electrostatic potentials and partial atomic charges were calculated for S-nitrosylated and unmodified cysteine residues. All three proteins are large multimeric enzymes in which pairs of equivalent modifiable cysteine residues from different monomers are arranged with their side chains in an antiparallel fashion across from each other. In mitochondrial aspartate aminotransferase, each cysteine residue at position 106 between chains A and B and C and D are 26 Å apart. In glutamate dehydrogenase, each cysteine residue at position 112 between chains A and E, B and E, and C and F is 20 Å apart, whereas cysteine residues 99 and 183 in glutamine synthetase between the side chains are about 23 Å apart. S-nitrosylation of the cysteine residue makes the side chain significantly more polar, increasing the dipole moment from 1.7 to 5.4 D. This increase in polarity results in an augmented electrostatic potential which, because of the antiparallel dipole arrangement and the effective propagation of electrostatic potentials inside large proteins (*52*–*61*), produces a repulsive electrostatic "wedge" between subunits (fig. S5). This wedge could drive changes in the quaternary structure and provide a plausible allosteric mechanism by which S-nitrosylation of cysteine residues distant from substrate and cofactor binding sites modulates enzyme activity.

DISCUSSION

S-nitrosylation of cysteine residues represents an alternative signaling mechanism through which NO can expand the functional diversity and biological use of proteins. We applied a combination of chemical enrichment and mass spectrometric technologies to specifically map endogenous sites of S-nitrosylation in wild-type, $nNOS^{-/-}$, and $eNOS^{-/-}$ mouse forebrain. In wild-type brain, 45 sites of S-nitrosylation in 44 proteins identified by our method have been previously reported with various biochemical and proteomic approaches. The current study contributed 225 additional S-nitrosylation sites as well as 92 additional protein targets, expanding the known endogenous S-nitrosylated proteins in the mouse brain. As with any enrichment method, the identification of the endogenous sites of S-nitrosylation is limited by the relative abundance and biological stability of *S*-nitrosocysteine. Despite these limitations, interrogation of the proteomic data coupled with biochemical approaches provided evidence that protein S-nitrosylation participates in the coordination of glutamate metabolism and neurotransmission. Specifically, four proteins that regulate glutamate uptake, metabolism, and conversion to glutamine are functionally regulated by S-nitrosylation.

Glutamate uptake through excitatory amino acid transporter 2, the major astrocytic transporter of glutamate in the CNS, was reversibly inhibited by S-nitrosylation at Cys^{373} and Cys^{562}. Irreversible alkylation of Cys^{373} inhibits transporter activity (*62*), whereas the functional role of Cys^{562} in the rat or Cys^{561} in the mouse has not been studied. Because permissive mutation of these two cysteine residues to serine did not alter the activity of excitatory amino acid transporter 2, these data suggest that both cysteine residues are not critical for function but that posttranslational modifications at these residues are important for functional regulation. We speculate that the transient inhibition of the transporter may allow for an extended period of increased glutamate concentration within the synaptic cleft, promoting neurotransmission and synaptic strengthening. The absence of nNOS-dependent S-nitrosylation of excitatory amino acid transporter 2 may prevent $nNOS^{-/-}$ mice from achieving this regulation and thereby contribute to their phenotype of dysregulated glutamatergic transmission, synaptic plasticity, and memory (*6*–*14*).

Metabolic studies have indicated that once in astrocytes, a fraction of glutamate (estimates vary from 50 to 70%) is converted to glutamine by glutamine synthetase (*63*, *64*). The remaining glutamate in astrocytes is oxidized by glutamate dehydrogenase and mitochondrial aspartate aminotransferase to α-ketoglutarate, which can then enter the tricarboxylic acid (TCA) cycle (*65*, *66*). The metabolic demands placed on astrocytes and neurons may determine the fraction of glutamate that is oxidized in the TCA cycle. Our data indicate that S-nitrosylation inhibited glutamate oxidation by glutamate dehydrogenase and mitochondrial aspartate aminotransferase, and promoted conversion to glutamine by glutamine synthetase (Fig. 2D). Moreover, the absence of S-nitrosylation of these enzymes in $nNOS^{-/-}$ mice resulted in a higher ratio of glutamine to glutamate, consistent with increased glutamate oxidation (Fig. 2, B and C). The lower fraction of glutamate converted to glutamine may contribute to the phenotype of the $nNOS^{-/-}$ mice. Although there are disagreements on the fraction of the re-cycled glutamate that participates in neurotransmission, genetic ablation of enzymes in the glutamate/glutamine cycle underscores the importance of maintaining this cycle in the CNS (*67*). Specifically, glutamine synthetase haploinsufficiency leads to increased seizure susceptibility in vivo (*68*), with complete deletion of the gene associated with decreased cortical glutamine and severely limited postnatal viability (*69*). Glutamate dehydrogenase deletion in vivo leads to increased glutamine concentrations in the brain (*70*), whereas overexpression of the enzyme leads to decreased synaptic plasticity and age-dependent loss of synaptic and dendritic architecture (*71*). During periods of increased synaptic activity, the effect of S-nitrosylation on the reallocation of glutamate from oxidation to regeneration of glutamine (and subsequent glutamate) provides an explanation for how sustained neurotransmission may be achieved in wild-type mice but not in $nNOS^{-/-}$ mice. The S-nitrosylation–induced alteration in glutamate metabolism could also explain why $nNOS^{-/-}$ mice are protected from cerebral ischemia (*15*). Our data suggest that neurons in the $nNOS^{-/-}$ brain would avidly oxidize glutamate and consequently exhibit attenuation of the ischemia-induced increase in intra-synaptic glutamate (*15*–*17*, *72*) while providing adenosine 5′-triphosphate (ATP) for metabolic processes. The partial loss of glutamine synthetase activity in $nNOS^{-/-}$ brain would hinder glutamate conversion to glutamine (an important mechanism of glutamate disposal) but would also spare limited reserves of ATP during an ischemic episode, because the glutamine synthetase pathway normally consumes considerable energy (*73*). Collectively, S-nitrosylation of these proteins may provide a regulatory switch between glutamate oxidation

and glutamine generation to support synaptic maintenance and glutamatergic neurotransmission.

Finally, it is interesting to note that of the 136 proteins identified as targets of S-nitrosylation in the wild-type mouse brain, 23 have been identified as part of macromolecular complexes implicated in glutamate metabolism at synapses (*74*). The association of glutamate uptake and mitochondrial mobility (*75*), the functional interaction between glutamate dehydrogenase–mediated glutamate oxidation and excitatory amino acid transporter 2–mediated glutamate uptake (*76*), and the data presented in Figs. 2 and 3 indicate that selective protein S-nitrosylation may function as a synapse-specific gatekeeper of glutamate fate during neurotransmission.

MATERIALS AND METHODS

Chemicals and reagents

Chemicals were purchased from Sigma-Aldrich unless otherwise indicated. Rabbit polyclonal antibody against excitatory amino acid transporter 2 was a gift from J. Rothstein (Johns Hopkins University School of Medicine, Baltimore, MD). Goat polyclonal antibodies against mitochondrial aspartate aminotransferase and glutamate dehydrogenase were purchased from Abcam. Mouse monoclonal antibody against glutamine synthetase was purchased from Millipore. L-[3,4-^{3}H] glutamic acid was purchased from Perkin-Elmer. Affi-Gel 10 was purchased from Bio-Rad. EZ-Link Sulfo-NHS-Biotin and UltraLink Monomeric Avidin beads were purchased from Pierce.

Animals

All procedures were performed in strict accordance with the National Institutes of Health *Guide for the Care and Use of Laboratory Animals* and were approved by the Children's Hospital of Philadelphia Animal Care and Use Committee. Male mice between 10 and 12 weeks old were used for proteomic studies, enzymatic assays, and synaptosomal uptake, whereas those between 8 and 10 weeks old were used for ^{15}N stable isotopic profiling. Wild-type C57BL/6J (#000664), *Nos1*^{tm1Unc} C57BL/6J (*nNOS*$^{-/-}$: #002986), and *Nos3*^{tm1Unc} C57BL/6J (*eNOS*$^{-/-}$: #002684) mice were obtained from Jackson Laboratories. For experiments, except those involving isotopic profiling, mice were anesthetized by CO_2 and perfused through the left ventricle with ice-cold phosphate-buffered saline (PBS). Intact organs were collected, immediately frozen in liquid nitrogen, and stored at −80°C until use.

Identification of protein *S*-nitrosocysteine sites

A detailed experimental procedure for the preparation and activation of columns, as well homogenate preparation for reaction with organic mercury resin, has been previously published (*30*). Six biological replicates from each genotype were analyzed. Each sample had a corresponding UV-pretreated negative control analyzed under identical conditions. The number of peptides identified in both untreated and UV-pretreated homogenates was used to calculate the false identification rate (FIR). The FIR was calculated independently for each biological replicate, and the average value is reported. Overall, the FIR across the six biological replicates was 5.2 ± 0.7%, which is within the range of FIR reported for site-specific identification of other posttranslational modifications using enrichment approaches (*77*, *78*). Columns were initially washed with 50 bed volumes of 50 mM tris-HCl (pH 7.4), containing 0.3 M NaCl, 0.5% SDS, followed by 50 bed volumes of the same buffer containing 0.05% SDS. Columns were then washed with 50 bed volumes of 50 mM tris-HCl pH 7.4, containing 0.3 M NaCl, 1% Triton X-100, 1 M urea. This was followed by 50 bed volumes of the same buffer containing 0.1% Triton X-100, 0.1 M urea. Finally, columns were washed with 200 bed volumes of water before proteins were eluted with 10 ml of 50 mM β-mercaptoethanol in water. Samples were concentrated and resolved by one-dimensional SDS–polyacrylamide gel electrophoresis (SDS-PAGE), followed by either Western blot analysis or in-gel trypsinization and subsequent liquid chromatography–tandem MS (LC-MS/MS) analysis (*28–30*, *79*).

For quantification of S-nitrosylated glutamate transporter type I, glutamate dehydrogenase, mitochondrial aspartate aminotransferase, and glutamine synthetase from wild-type mouse brain, the same protein capture protocol described above was followed. Equivalent fractions of the eluted bound proteins, representing the S-nitrosylated fraction, 30 μg of input homogenate (total protein), and different dilutions of recombinant standard proteins, were resolved by one-dimensional SDS-PAGE and transferred to Immobilon-FL PVDF (polyvinylidene fluoride) membranes (Millipore). After probing with appropriate antibodies, blots were scanned by the Odyssey Infrared Imaging System (LI-COR).

To identify sites of *S*-nitrosocysteines, columns were washed with 10 bed volumes of 0.1 M ammonium bicarbonate after the final wash with water in the previously described method. Bound proteins were subjected to digestion by the addition of Trypsin Gold (1 μg/ml) (Promega) in one bed volume of 0.1 M ammonium bicarbonate in the dark for 16 hours at room temperature. The resin was next washed with 40 bed volumes of 1 M ammonium bicarbonate, pH 7.4, containing 300 mM NaCl, followed by 40 volumes of the same buffer without NaCl. Columns were then washed with 40 volumes of 0.1 M ammonium bicarbonate followed by 200 volumes of deionized water. Performic acid was synthesized by reacting 1% formic acid and 0.5% hydrogen peroxide for at least 60 min at room temperature (with rocking) in a glass vial shielded from light. To elute bound peptides, the resin was incubated with one bed volume of performic acid in water for 30 min at room temperature (*28–30*). Eluted peptides were recovered by washing the resin with one bed volume of deionized water. Eluates were stored at −80°C overnight followed by lyophilization and resuspension into 300 μl of 0.1% formic acid. Peptide suspensions were transferred to low-retention tubes (Axygen), and the volume was reduced to 30 μl by speed vacuum. Twenty microliters of peptide suspension was transferred to an HPLC vial and submitted for LC-MS/MS analysis. The details for MS/MS analysis have been provided previously (*28–30*, *79*). Post-MS analysis to generate the *S*-nitrosocysteine proteomes (table S1) was performed as described previously (*28–30*). The peptides that are reported for the wild-type mice have been identified in at least three biological replicates.

GO analysis

Proteins in table S1 were mapped to UniProt IDs, and only reviewed, non-fragment proteins were retained in the final proteome. A mouse brain reference brain proteome consisting of 7025 proteins was generated from the literature (*31–34*) and our experimental data. For GO analysis, the *R* score was calculated by WebGestalt (*35*) as the ratio (*O*:*E*) of the observed number (*O*) of proteins with a specific GO annotation in the *S*-nitrosocysteine proteome versus the number of annotated proteins expected (*E*) to be in the *S*-nitrosocysteine proteome. *E* is derived from the number of proteins annotated as part of a specific molecular pathway in the whole-brain proteome normalized to the number of total proteins in the whole-brain protein proteome (and multiplied by the total number of S-nitrosylated proteins). Significant enrichment was evaluated at an adjusted cutoff of 0.01, with the top 10 enriched pathways considered for further analysis.

Glutamate/glutamine metabolism studies

For isotopic profiling studies, three mice per genotype were analyzed. Each day, samples from one mouse per genotype were prepared and analyzed. Animals were anesthetized with isoflurane and decapitated. The brain

was then rapidly removed, and coronal hippocampal slices (400 μm) were cut with a vibratome (Vibratome 1000 Plus, Vibratome) in an ice-cold artificial cerebrospinal fluid (ACSF) solution of the following composition: 202 mM sucrose, 3 mM KCl, 1.25 mM NaH_2PO_4, 26 mM $NaHCO_3$, 10 mM glucose, 1 mM $MgCl_2$, 2 mM $CaCl_2$, pH 7.2 to 7.4 (when saturated with 95% O_2–5% CO_2). Slices were then equilibrated for 2 hours at 34°C in ACSF containing 130 mM NaCl instead of sucrose. After equilibration, hippocampal slices were transferred into cell culture inserts and incubated in a 24-well plate for 45 min at 34°C in 1 ml of depolarizing artificial cerebrospinal fluid containing the following: 130 mM NaCl, 3 mM KCl, 1.25 mM NaH_2PO_4, 26 mM $NaHCO_3$, 10 mM glucose, 2 mM $CaCl_2$, 1 mM [2-^{15}N] L-glutamine, and 0.3 mM NH_4Cl. Medium was then collected from each sample and frozen at −80°C, and slices were washed with 2 ml of chilled Dulbecco's PBS (DPBS). Slices were homogenized in 4% perchloric acid and subjected to two freeze/thaw cycles, with a subsequent centrifugation step at 10,000*g* for 15 min. Supernatant was collected from each slice, which contained the metabolites of interest, and protein pellets were separately resuspended in 1 M NaOH. Protein content per slice was determined using the Bio-Rad Protein Assay. Supernatant from each sample was neutralized with KOH and used for metabolite determination and measurement of ^{15}N enrichment by GC-MS (*40*, *41*).

Enzymatic assays

For enzymatic activities, three mice per genotype were analyzed. Each day, three mice (one mouse per genotype) were analyzed. Enzymatic activities were quantified in triplicates with technical reproducibility greater than 90%. Afterward, the average raw values were normalized to those of untreated wild-type homogenate analyzed the same day.

For glutamine synthetase activity, frozen tissues from mouse brain cortex were processed as described previously (*80*) with minor modifications. Briefly, cortices were homogenized in five volumes of 0.1 M imidazole (pH 7.2) using an ULTRA-TURRAX homogenizer. Homogenates were centrifuged at 10,000*g* for 10 min at 4°C, and the clarified supernatant was used for assessing glutamine synthetase activity (with protein concentration determined using the Bio-Rad Protein Assay). For UV light exposure to eliminate NO from *S*-nitrosocysteine, part of each sample from wild-type mice was trans-illuminated by UV light while on ice for 3 min. Activity was determined in triplicate using 90 μg of clarified homogenate in a total volume of 70 μl of reaction buffer [1 mM L-glutamate, 20 mM ATP, 40 mM $MgCl_2$, 0.1 M hydroxylamine, 0.1 M imidazole (pH 7.2)] after incubation for 20 min at 37°C. The reaction was stopped by the addition of 190 μl of 0.37 M $FeCl_3$ in 0.67 M HCl/0.2 M TCA, and samples were incubated on ice for 5 min. Sample mixtures were then centrifuged at 4°C for 5 min at 10,000*g*, and the absorbance of the resulting supernatant was measured at 535 nm and compared to a standard curve of authentic L-glutamylhydroxamate. Glutamine synthetase activity was expressed as nanomole of L-glutamylhydroxamate per milligram of protein per hour. Enzymatic specificity of the assay was determined using 0.5 mM MSO as a selective glutamine synthetase inhibitor.

For glutamate dehydrogenase activity, frozen forebrain was processed using the Mitochondrial Isolation Kit from Sigma-Aldrich. The final mitochondrial pellet was resuspended in mitochondrial resuspension buffer containing 0.32 M sucrose, 10 mM tris-HCl (pH 7.4), 0.5 mM EDTA, 0.1% Triton X-100, and protein concentration was determined using the Bio-Rad Protein Assay. Glutamate dehydrogenase activity was determined as described previously (*81*). Briefly, activity in the direction of oxidative deamination was assayed in a UV/Visible spectrophotometer (HP 8452A, GMI Inc.) at 25°C using 15 μg of mitochondrial protein in a final volume of 200 μl of assay buffer [150 mM KCl, 0.1 mM rotenone, 20 mM tris-HCl (pH 7.6), 2 mM EGTA, 1 mM NAD^+ (nicotinamide adenine dinucleotide), 2.5 mM glutamate]. The velocity of each reaction was calculated from the linear portion of the change in NADH (reduced form of NAD^+) absorbance measured at 340 nm. Enzymatic specificity of the assay was determined using 20 μM GTP as a selective glutamate dehydrogenase inhibitor.

For mitochondrial aspartate aminotransferase activity, mitochondrial extracts were prepared exactly as described for glutamate dehydrogenase activity. Enzymatic activity was determined as described previously (*82*), with minor modifications. Briefly, activity in the direction of α-ketoglutarate production was assayed spectrophotometrically using 15 μg of mitochondrial protein in a final volume of 200 μl of assay buffer [0.02% BSA (bovine serum albumin), 0.1 mM rotenone, 100 mM ADP (adenosine 5′-diphosphate), 30 mM NH_4Cl, 120 μM NADPH (reduced form of $NADP^+$), 5 mM Glu, 2.5 mM oxaloacetic acid, and 15 μg of purified bovine glutamate dehydrogenase]. The decrease in NADPH absorbance at 340 nm at room temperature was followed over 15 min and used to calculate the velocity of mitochondrial aspartate aminotransferase activity. Enzymatic specificity of the assay was determined using 1 mM AOAA as a selective inhibitor of mitochondrial aspartate aminotransferase.

For synaptosomal glutamate uptake, crude synaptosomes were prepared from forebrain as previously described (*49*, *83*) with minor modifications. Briefly, animals between 10 and 12 weeks of age were anesthetized with isoflurane and decapitated. Forebrains from wild-type, *nNOS*$^{-/-}$, and *eNOS*$^{-/-}$ mice were dissected and homogenized on ice in 20 volumes of sucrose buffer [0.32 M sucrose, 0.1 mM DTPA (diethylenetriamine pentaacetic acid), pH 5.3] while protected from light. Homogenates were centrifuged at 800*g* for 10 min at 4°C, and the supernatants were isolated for further processing. Samples from wild-type mice homogenized in sucrose buffer without DTPA were also pretreated at 4°C with 50 μM $CuSO_4$/500 μM ascorbate for 30 min in the dark to remove NO from *S*-nitrosocysteine. All samples were then centrifuged at 20,000*g* for 20 min at 4°C, and the pellets were resuspended in 0.32 M sucrose, 0.1 mM DTPA (pH 5.3). Samples were then centrifuged a final time at 20,000*g* for 20 min at 4°C, with pellets finally resuspended in 0.32 M sucrose (pH 5.3). Sodium-dependent transport of L-^{3}[H]glutamate was then measured as described previously (*49*, *83*) in the presence or absence of 0.3 mM DHK to determine DHK-sensitive glutamate uptake (as a measure of excitatory amino acid transporter 2 activity).

Plasmid constructs

Plasmid expressing rat excitatory amino acid transporter 2 was obtained from B. Kanner (Hebrew University, Hadassah Medical School, Jerusalem, Israel). The QuikChange Lightning Site-Directed Mutagenesis Kit (Agilent Technologies) was used to introduce single amino acid mutations in the transporter as follows. Cysteine-to-serine mutations were introduced using the forward/reverse primer pairs: for Cys^{373}, 5′-TTGCCTGTCACCTTCCGTAGCTTGGAAGATAATC-3′ and 5′-GATTATCTTCCAAGCTACGGAAGGTGACAGGCAA-3′; and for Cys^{562}, 5′- ATGGAAAGTCAGCTGACAGCAGTGTTGAGGAAGAA-3′ and 5′- TTCTTCCTCAACACTGCTGTCAGCTGACTTTCCAT-3′, resulting in the C373S/C562S construct. All plasmid constructs were verified by sequencing before use.

Cell culture, transfection, and CysNO treatment

HEK-293T cells were grown in Dulbecco's modified Eagle's medium (DMEM) with GlutaMAX from Life Technologies containing 10% fetal bovine serum, penicillin (100 U/ml), and streptomycin (100 ng/ml), at 37°C in air with 5% CO_2. Cells were plated at a density of 1.25×10^5 cells/cm^2 and cultured under normal conditions for 24 hours. Cells were transfected with wild-type excitatory amino acid transporter 2 or the double mutant

(C373S/C562S) transporter using the Clontech CalPhos transfection kit according to the manufacturer's protocol. At 18 hours posttransfection, the growth medium was replaced with serum-free DMEM and equilibrated for 2 hours at 37°C. Afterward, freshly prepared *S*-nitrosocysteine (CysNO) or cysteine (Cys) was added up to a final concentration of 0.4 mM, and cells were incubated for 2 hours. Cells were extensively washed with PBS and used for measuring glutamate uptake as described previously (*84*). Lysates were assayed for protein concentration using the Lowry assay and used to determine excitatory amino acid transporter 2–mediated glutamate uptake initial velocity, described in nanomole per milligram per minute. For cell surface biotinylation studies, cells were processed as described previously (*84*). Briefly, after Cys or CysNO treatment, cell monolayers were washed twice with ice-cold DPBS (pH 7.4) containing 0.1 mM $CaCl_2$ and 1.0 mM $MgCl_2$. Cells were then incubated in 2 ml of biotinylation solution [EZ-Link Sulfo-NHS-Biotin (1 mg/ml) in DPBS with 0.1 mM $CaCl_2$ and 1.0 mM $MgCl_2$] for 30 min at 4°C. The biotinylation solution was then aspirated, and excess biotin was quenched by incubating cells with DPBS containing 100 mM glycine for 30 min at 4°C. Cells were then lysed in 1 ml radioimmunoprecipitation assay buffer with protease inhibitors [leupeptin (1 μg/ml), 250 μM phenylmethanesulfonyl fluoride, aprotinin (1 μg/ml), and 1 mM iodoacetamide]. Lysates were then centrifuged to remove cellular debris, and biotinylated proteins were batch extracted from the supernatant using UltraLink Monomeric Avidin beads. Lithium dodecyl sulfate (LDS) sample buffer was added to fractions containing total cell lysate, biotinylated proteins (cell surface proteins), and nonbiotinylated proteins (intracellular proteins). Each fraction was diluted and loaded such that the sum of immunoreactivity in the nonbiotinylated and biotinylated fractions should equal the immunoreactivity found in the lysate, assuming avidin extraction of biotinylated proteins is 100%. For reversibility studies, uptake was studied in cells at 0, 60, 120, and 240 min after the removal of CysNO. Additionally, lysates from each treatment condition were processed in parallel, as previously described (*28*–*30*), for S-nitrosoprotein enrichment and subsequent Western blot detection of S-nitrosylated excitatory amino acid transporter 2.

Molecular modeling of the effects of S-nitrosylation

The 2.4-Å resolution crystal structure of mitochondrial aspartate aminotransferase was taken from PDB 3PD6 (*53*). The 2.7-Å resolution crystal structure of human glutamate dehydrogenase was taken from PDB 1L1F (*54*). The 2.6-Å resolution crystal structure of human glutamine synthetase was taken from PDB 2QC8 (*55*). Structures of mitochondrial aspartate aminotransferase with S-nitrosyl–modified cysteine (SNC) at positions 106 and 295, glutamate dehydrogenase with SNC at position 59 (equivalent to position 112 in the mouse sequence), and glutamate synthetase with SNC at positions 99, 183, 269, and 346 were built using Visual Molecular Dynamics (VMD) and a custom SNC residue template (*56*). Electrostatic potentials from the cysteine or SNC residues were calculated using the finite difference Poisson-Boltzmann method as described previously (*57*, *58*). The solvent was assigned a dielectric of 78.6 and an ionic strength of 145 mM. The protein was assigned a dielectric of 2. Partial atomic charges for the unmodified cysteine residue were taken from the CHARMM27 molecular mechanics force field (*59*). Atomic charges for SNC were obtained from electronegativity neutralization using the program QEQUIL (*60*), giving +0.35 ($C_\beta H_2$), −0.17 (S_γ), +0.06 (N_δ), and −0.24 (O_ε), in atomic charge units. Structures and potentials were visualized using PyMol (*61*).

Statistical analysis

Data were analyzed with GraphPad Prism 5.0d software. All normally distributed data were displayed as means ± SE. Groups were analyzed by one- or two-way ANOVA, with appropriate post hoc tests.

SUPPLEMENTARY MATERIALS

www.sciencesignaling.org/cgi/content/full/8/384/ra68/DC1

Fig. S1. Reduction in the enrichment of S-nitrosylated proteins in *eNOS*$^{-/-}$ and *nNOS*$^{-/-}$ mice.

Fig. S2. Additional biological processes and cellular functions identified for S-nitrosylated proteins in the mouse brain.

Fig. S3. Identification of ^{15}N isotopic label in glutamate-associated metabolites.

Fig. S4. Characterization of GLT1-independent uptake in synaptosomes and GLT1-dependent uptake in cells.

Fig. S5. S-nitrosylation augments electrostatic potential.

Table S1. *S*-nitrosocysteine sites identified in wild-type, *eNOS*$^{-/-}$, and *nNOS*$^{-/-}$ mouse brain.

REFERENCES AND NOTES

1. E. M. Schuman, D. V. Madison, A requirement for the intercellular messenger nitric oxide in long-term potentiation. *Science* **254**, 1503–1506 (1991).
2. J. E. Haley, G. L. Wilcox, P. F. Chapman, The role of nitric oxide in hippocampal long-term potentiation. *Neuron* **8**, 211–216 (1992).
3. T. J. O'Dell, P. L. Huang, T. M. Dawson, J. L. Dinerman, S. H. Snyder, E. R. Kandel, M. C. Fishman, Endothelial NOS and the blockade of LTP by NOS inhibitors in mice lacking neuronal NOS. *Science* **265**, 542–546 (1994).
4. H. Son, R. D. Hawkins, K. Martin, M. Kiebler, P. L. Huang, M. C. Fishman, E. R. Kandel, Long-term potentiation is reduced in mice that are doubly mutant in endothelial and neuronal nitric oxide synthase. *Cell* **87**, 1015–1023 (1996).
5. P. L. Huang, T. M. Dawson, D. S. Bredt, S. H. Snyder, M. C. Fishman, Targeted disruption of the neuronal nitric oxide synthase gene. *Cell* **75**, 1273–1286 (1993).
6. K. M. Kendrick, R. Guevara-Guzman, J. Zorrilla, M. R. Hinton, K. D. Broad, M. Mimmack, S. Ohkura, Formation of olfactory memories mediated by nitric oxide. *Nature* **388**, 670–674 (1997).
7. R. Weitzdoerfer, H. Hoeger, E. Engidawork, M. Engelmann, N. Singewald, G. Lubec, B. Lubec, Neuronal nitric oxide synthase knock-out mice show impaired cognitive performance. *Nitric Oxide* **10**, 130–140 (2004).
8. M. Jüch, K. H. Smalla, T. Kähne, G. Lubec, W. Tischmeyer, E. D. Gundelfinger, M. Engelmann, Congenital lack of nNOS impairs long-term social recognition memory and alters the olfactory bulb proteome. *Neurobiol. Learn. Mem.* **92**, 469–484 (2009).
9. S. P. Zoubovsky, V. M. Pogorelov, Y. Taniguchi, S.-H. Kim, P. Yoon, E. Nwulia, A. Sawa, M. V. Pletnikov, A. Kamiya, Working memory deficits in neuronal nitric oxide synthase knockout mice: Potential impairments in prefrontal cortex mediated cognitive function. *Biochem. Biophys. Res. Commun.* **408**, 707–712 (2011).
10. J. R. Steinert, C. Kopp-Scheinpflug, C. Baker, R. A. Challiss, R. Mistry, M. D. Haustein, S. J. Griffin, H. Tong, B. P. Graham, I. D. Forsythe, Nitric oxide is a volume transmitter regulating postsynaptic excitability at a glutamatergic synapse. *Neuron* **60**, 642–656 (2008).
11. G. A. Rameau, D. S. Tukey, E. D. Garcin-Hosfield, R. F. Titcombe, C. Misra, L. Khatri, E. D. Getzoff, E. B. Ziff, Biphasic coupling of neuronal nitric oxide synthase phosphorylation to the NMDA receptor regulates AMPA receptor trafficking and neuronal cell death. *J. Neurosci.* **27**, 3445–3455 (2007).
12. S. Blackshaw, M. J. Eliasson, A. Sawa, C. C. Watkins, D. Krug, A. Gupta, T. Arai, R. J. Ferrante, S. H. Snyder, Species, strain and developmental variations in hippocampal neuronal and endothelial nitric oxide synthase clarify discrepancies in nitric oxide-dependent synaptic plasticity. *Neuroscience* **119**, 979–990 (2003).
13. J. Dachtler, N. R. Hardingham, S. Glazewski, N. F. Wright, E. J. Blain, K. Fox, Experience-dependent plasticity acts via GluR1 and a novel neuronal nitric oxide synthase-dependent synaptic mechanism in adult cortex. *J. Neurosci.* **31**, 11220–11230 (2011).
14. M. D. Lange, M. Doengi, J. Lesting, H. C. Pape, K. Jüngling, Heterosynaptic long-term potentiation at interneuron–principal neuron synapses in the amygdala requires nitric oxide signalling. *J. Physiol.* **590**, 131–143 (2012).
15. Z. Huang, P. L. Huang, N. Panahian, T. Dalkara, M. C. Fishman, M. A. Moskowitz, Effects of cerebral ischemia in mice deficient in neuronal nitric oxide synthase. *Science* **265**, 1883–1885 (1994).
16. R. Sattler, Z. Xiong, W. Y. Lu, M. Hafner, J. F. MacDonald, M. Tymianski, Specific coupling of NMDA receptor activation to nitric oxide neurotoxicity by PSD-95 protein. *Science* **284**, 1845–1848 (1999).
17. T. Kleppisch, A. Pfeifer, P. Klatt, P. Ruth, A. Montkowski, R. Fassler, F. Hofmann, Long-term potentiation in the hippocampal CA1 region of mice lacking cGMP-dependent kinases is normal and susceptible to inhibition of nitric oxide synthase. *J. Neurosci.* **19**, 48–55 (1999).
18. S. Jacoby, R. E. Sims, N. A. Hartell, Nitric oxide is required for the induction and heterosynaptic spread of long-term potentiation in rat cerebellar slices. *J. Physiol.* **535**, 825–839 (2001).
19. V. Lev-Ram, S. T. Wong, D. R. Storm, R. Y. Tsien, A new form of cerebellar long-term potentiation is postsynaptic and depends on nitric oxide but not cAMP. *Proc. Natl. Acad. Sci. U.S.A.* **99**, 8389–8393 (2002).

20. S. R. Jaffrey, H. Erdjument-Bromage, C. D. Ferris, P. Tempst, S. H. Snyder, Protein S-nitrosylation: A physiological signal for neuronal nitric oxide. *Nat. Cell Biol.* **3**, 193–197 (2001).
21. Y.-B. Choi, L. Tenneti, D. A. Le, J. Ortiz, G. Bai, H.-S. Chen, S. A. Lipton, Molecular basis of NMDA receptor-coupled ion channel modulation by S-nitrosylation. *Nat. Neurosci.* **3**, 15–21 (2000).
22. B. Selvakumar, M. A. Jenkins, N. K. Hussain, R. L. Huganir, S. F. Traynelis, S. H. Snyder, S-nitrosylation of AMPA receptor GluA1 regulates phosphorylation, single-channel conductance, and endocytosis. *Proc. Natl. Acad. Sci. U.S.A.* **110**, 1077–1082 (2013).
23. G. P. H. Ho, B. Selvakumar, J. Mukai, L. D. Hester, Y. Wang, J. A. Gogos, S. H. Snyder, S-nitrosylation and S-palmitoylation reciprocally regulate synaptic targeting of PSD-95. *Neuron* **71**, 131–141 (2011).
24. B. Dejanovic, G. Schwarz, Neuronal nitric oxide synthase-dependent S-nitrosylation of gephyrin regulates gephyrin clustering at GABAergic synapses. *J. Neurosci.* **34**, 7763–7768 (2014).
25. Y. Huang, H.-Y. Man, Y. Sekine-Aizawa, Y. Han, K. Juluri, H. Luo, J. Cheah, C. Lowenstein, R. L. Huganir, S. H. Snyder, S-nitrosylation of N-ethylmaleimide sensitive factor mediates surface expression of AMPA receptors. *Neuron* **46**, 533–540 (2005).
26. B. Selvakumar, R. L. Huganir, S. H. Snyder, S-nitrosylation of stargazin regulates surface expression of AMPA-glutamate neurotransmitter receptors. *Proc. Natl. Acad. Sci. U.S.A.* **106**, 16440–16445 (2009).
27. A. K. Mustafa, M. Kumar, B. Selvakumar, G. P. H. Ho, J. T. Ehmsen, R. K. Barrow, L. M. Amzel, S. H. Snyder, Nitric oxide *S*-nitrosylates serine racemase, mediating feedback inhibition of D-serine formation. *Proc. Natl. Acad. Sci. U.S.A.* **104**, 2950–2955 (2007).
28. P.-T. Doulias, J. L. Greene, T. M. Greco, M. Tenopoulou, S. H. Seeholzer, R. L. Dunbrack, H. Ischiropoulos, Structural profiling of endogenous S-nitrosocysteine residues reveals unique features that accommodate diverse mechanisms for protein S-nitrosylation. *Proc. Natl. Acad. Sci. U.S.A.* **107**, 16958–16963 (2010).
29. P.-T. Doulias, M. Tenopoulou, J. L. Greene, K. Raju, H. Ischiropoulos, Nitric oxide regulates mitochondrial fatty acid metabolism through reversible protein S-nitrosylation. *Sci. Signal.* **6**, rs1 (2013).
30. P.-T. Doulias, M. Tenopoulou, K. Raju, L. A. Spruce, S. H. Seeholzer, H. Ischiropoulos, Site specific identification of endogenous S-nitrosocysteine proteomes. *J. Proteomics* **92**, 195–203 (2013).
31. T. Kislinger, B. Cox, A. Kannan, C. Chung, P. Hu, A. Ignatchenko, M. S. Scott, A. O. Gramolini, Q. Morris, M. T. Hallett, J. Rossant, T. R. Hughes, B. Frey, A. Emili, Global survey of organ and organelle protein expression in mouse: Combined proteomic and transcriptomic profiling. *Cell* **125**, 173–186 (2006).
32. E. L. Huttlin, M. P. Jedrychowski, J. E. Elias, T. Goswami, R. Rad, S. A. Beausoleil, J. Villén, W. Haas, M. E. Sowa, S. P. Gygi, A tissue-specific atlas of mouse protein phosphorylation and expression. *Cell* **143**, 1174–1189 (2010).
33. H. Wang, W. J. Qian, M. H. Chin, V. A. Petyuk, R. C. Barry, T. Liu, M. A. Gritsenko, H. M. Mottaz, R. J. Moore, D. G. Camp Ii, A. H. Khan, D. J. Smith, R. D. Smith, Characterization of the mouse brain proteome using global proteomic analysis complemented with cysteinyl-peptide enrichment. *J. Proteome Res.* **5**, 361–369 (2006).
34. L. Martens, M. Müller, C. Stephan, M. Hamacher, K. A. Reidegeld, H. E. Meyer, M. Blüggel, J. Vandekerckhove, K. Gevaert, R. Apweiler, A comparison of the HUPO Brain Proteome Project pilot with other proteomics studies. *Proteomics* **6**, 5076–5086 (2006).
35. J. Wang, D. Duncan, Z. Shi, B. Zhang, WEB-based GEne SeT AnaLysis Toolkit (WebGestalt): Update 2013. *Nucleic Acids Res.* **41**, W77–W83 (2013).
36. D. L. Rothman, K. L. Behar, F. Hyder, R. G. Shulman, In vivo NMR studies of the glutamate neurotransmitter flux and neuroenergetics: Implications for brain function. *Annu. Rev. Physiol.* **65**, 401–427 (2003).
37. B. Pardo, T. B. Rodrigues, L. Contreras, M. Garzon, I. Llorente-Folch, K. Kobayashi, T. Saheki, S. Cerdan, J. Satrustegui, Brain glutamine synthesis requires neuronal-born aspartate as amino donor for glial glutamate formation. *J. Cereb. Blood Flow Metab.* **31**, 90–101 (2011).
38. L. Hertz, The glutamate–glutamine (GABA) cycle: Importance of late postnatal development and potential reciprocal interactions between biosynthesis and degradation. *Front. Endocrinol.* **4**, 59 (2013).
39. A. Schousboe, L. K. Bak, H. S. Waagepetersen, Astrocytic control of biosynthesis and turnover of the neurotransmitters glutamate and GABA. *Front. Endocrinol.* **4**, 102 (2013).
40. I. Nissim, O. Horyn, I. Nissim, Y. Daikhin, S. L. Wehrli, M. Yudkoff, F. M. Matschinsky, Effects of a glucokinase activator on hepatic intermediary metabolism: Study with ^{13}C-isotopomer-based metabolomics. *Biochem. J.* **444**, 537–551 (2012).
41. I. Nissim, E. Brosnan, M. Yudkoff, I. Nissim, J. B. Brosnan, Insulin and glucagon regulation of hepatic glutamine kinetics and metabolism: Studies in perfused liver with ^{15}N-labeled glutamine. *J. Biol. Chem.* **274**, 28958–28965 (1999).
42. M. T. Forrester, M. W. Foster, J. S. Stamler, Assessment and application of the biotin switch technique for examining protein S-nitrosylation under conditions of pharmacologically induced oxidative stress. *J. Biol. Chem.* **282**, 13977–13983 (2007).
43. B. Derakhshan, P. C. Wille, S. S. Gross, Unbiased identification of cysteine S-nitrosylation sites on proteins. *Nat. Protoc.* **2**, 1685–1691 (2007).
44. W. B. Rowe, R. A. Ronzio, A. Meister, Inhibition of glutamine synthetase by methionine sulfoximine. Studies on methionine sulfoximine phosphate. *Biochemistry* **8**, 2674–2680 (1969).
45. Ø. Haugeto, K. Ullensvang, L. M. Levy, F. A. Chaudhry, T. Honoré, M. Nielsen, K. P. Lehre, N. C. Danbolt, Brain glutamate transporter proteins form homomultimers. *J. Biol. Chem.* **271**, 27715–27722 (1996).
46. J. D. Rothstein, M. Dykes-Hoberg, C. A. Pardo, L. A. Bristol, L. Jin, R. W. Kuncl, Y. Kanai, M. A. Hediger, Y. Wang, J. P. Schielke, D. F. Welty, Knockout of glutamate transporters reveals a major role for astroglial transport in excitotoxicity and clearance of glutamate. *Neuron* **16**, 675–686 (1996).
47. K. Tanaka, K. Watase, T. Manabe, K. Yamada, M. Watanabe, K. Takahashi, H. Iwama, T. Nishikawa, N. Ichihara, T. Kikuchi, S. Okuyama, N. Kawashima, S. Hori, M. Takimoto, K. Wada, Epilepsy and exacerbation of brain injury in mice lacking the glutamate transporter GLT-1. *Science* **276**, 1699–1702 (1997).
48. J. D. Pita-Almenar, S. Zou, C. M. Colbert, A. Eskin, Relationship between increase in astrocytic GLT-1 glutamate transport and late-LTP. *Learn. Mem.* **19**, 615–626 (2012).
49. M. B. Robinson, Examination of glutamate transporter heterogeneity using synaptosomal preparations. *Methods Enzymol.* **296**, 189–202 (1998).
50. X. Wang, N. J. Kettenhoffen, S. Shiva, N. Hogg, M. T. Gladwin, Copper dependence of the biotin switch assay: Modified assay for measuring cellular and blood nitrosated proteins. *Free Radic. Biol. Med.* **44**, 1362–1372 (2008).
51. Y. Zhang, N. Hogg, *S*-nitrosothiols: Cellular formation and transport. *Free Radic. Biol. Med.* **38**, 831–838 (2005).
52. J. Zhang, M. R. Gunner, Multiconformation continuum electrostatics analysis of the effects of a buried Asp introduced near heme *a* in *Rhodobacter sphaeroides* cytochrome *c* oxidase. *Biochemistry* **49**, 8043–8052 (2010).
53. Q. Han, H. Robinson, T. Cai, D. A. Tagle, J. Li, Biochemical and structural characterization of mouse mitochondrial aspartate aminotransferase, a newly identified kynurenine aminotransferase-IV. *Biosci. Rep.* **31**, 323–332 (2011).
54. T. J. Smith, T. Schmidt, J. Fang, J. Wu, G. Siuzdak, C. A. Stanley, The structure of apo human glutamate dehydrogenase details subunit communication and allostery. *J. Mol. Biol.* **318**, 765–777 (2002).
55. W. W. Krajewski, R. Collins, L. Holmberg-Schiavone, T. A. Jones, T. Karlberg, S. L. Mowbray, Crystal structures of mammalian glutamine synthetases illustrate substrate-induced conformational changes and provide opportunities for drug and herbicide design. *J. Mol. Biol.* **375**, 217–228 (2008).
56. W. Humphrey, A. Dalke, K. Schulten, VMD: Visual molecular dynamics. *J. Molec. Graph.* **14**, 33–38 (1996).
57. A.-S. Yang, M. R. Gunner, R. Sampogna, K. Sharp, B. Honig, On the calculation of pK_as in proteins. *Proteins* **15**, 252–265 (1993).
58. K. A. Sharp, Electrostatic interactions in hirudin-thrombin binding. *Biophys. Chem.* **61**, 37–49 (1996).
59. A. D. MacKerell Jr., B. Brooks, C. L. Brooks III, L. Nilsson, B. Roux, Y. Won, M. Karplus in *The Encyclopedia of Computational Chemistry*, P.v.R. Schleyer, Ed. (John Wiley & Sons, Chichester, 1998), pp. 271–277.
60. Q. Yang, K. A. Sharp, Atomic charge parameters for the finite difference Poisson-Boltzmann method using electronegativity neutralization. *J. Chem. Theory Comput.* **2**, 1152–1167 (2006).
61. W. L. DeLano, *The PyMOL Molecular Graphics System* (DeLano Scientific, San Carlos, CA, 2002).
62. M. Grunewald, D. Menaker, B. I. Kanner, Cysteine-scanning mutagenesis reveals a conformationally sensitive reentrant pore-loop in the glutamate transporter GLT-1. *J. Biol. Chem.* **277**, 26074–26080 (2002).
63. V. Lebon, K. F. Petersen, G. W. Cline, J. Shen, G. F. Mason, S. Dufour, K. L. Behar, G. I. Shulman, D. L. Rothman, Astroglial contribution to brain energy metabolism in humans revealed by ^{13}C nuclear magnetic resonance spectroscopy: Elucidation of the dominant pathway for neurotransmitter glutamate repletion and measurement of astrocytic oxidative metabolism. *J. Neurosci.* **22**, 1523–1531 (2002).
64. J. Shen, K. F. Petersen, K. L. Behar, P. Brown, T. W. Nixon, G. F. Mason, O. A. Petroff, G. I. Shulman, R. G. Shulman, D. L. Rothman, Determination of the rate of the glutamate/glutamine cycle in the human brain by in vivo 13C NMR. *Proc. Natl. Acad. Sci. U.S.A.* **96**, 8235–8240 (1999).
65. M. C. McKenna, U. Sonnewald, X. Huang, J. Stevenson, H. R. Zielke, Exogenous glutamate concentration regulates the metabolic fate of glutamate in astrocytes. *J. Neurochem.* **66**, 386–393 (1996).
66. M. C. McKenna, Glutamate pays its own way in astrocytes. *Front. Endocrinol.* **4**, 191 (2013).
67. H. Tani, C. G. Dulla, Z. Farzampour, A. Taylor-Weiner, J. R. Huguenard, R. J. Reimer, A local glutamate-glutamine cycle sustains synaptic excitatory transmitter release. *Neuron* **81**, 888–900 (2014).
68. K. L. van Gassen, W. S. van der Hel, T. B. Hakvoort, W. H. Lamers, P. N. de Graan, Haploinsufficiency of glutamine synthetase increases susceptibility to experimental febrile seizures. *Genes Brain Behav.* **8**, 290–295 (2009).
69. Y. He, T. B. Hakvoort, J. L. Vermeulen, W. T. Labruyére, D. R. De Waart, W. S. Van Der Hel, J. M. Ruijter, H. B. Uylings, W. H. Lamers, Glutamine synthetase deficiency in murine astrocytes results in neonatal death. *Glia* **58**, 741–754 (2010).

70. F. Frigerio, M. Karaca, M. De Roo, V. Mlynárik, D. M. Skytt, S. Carobbio, K. Pajęcka, H. S. Waagepetersen, R. Gruetter, D. Muller, P. Maechler, Deletion of glutamate dehydrogenase 1 (Glud1) in the central nervous system affects glutamate handling without altering synaptic transmission. *J. Neurochem.* **123**, 342–348 (2012).
71. X. Bao, R. Pal, K. N. Hascup, Y. Wang, W. T. Wang, W. Xu, D. Hui, A. Agbas, X. Wang, M. L. Michaelis, I.-Y. Choi, A. B. Belousov, G. A. Gerhardt, E. K. Michaelis, Transgenic expression of *Glud1* (glutamate dehydrogenase 1) in neurons: In vivo model of enhanced glutamate release, altered synaptic plasticity, and selective neuronal vulnerability. *J. Neurosci.* **29**, 13929–13944 (2009).
72. T. Kano, M. Shimizu-Sasamata, P. L. Huang, M. A. Moskowitz, E. H. Lo, Effects of nitric oxide synthase gene knockout on neurotransmitter release in vivo. *Neuroscience* **86**, 695–699 (1998).
73. P. K. Maciejewski, D. L. Rothman, Proposed cycles for functional glutamate trafficking in synaptic neurotransmission. *Neurochem. Int.* **52**, 809–825 (2008).
74. E. N. Genda, J. G. Jackson, A. L. Sheldon, S. F. Locke, T. M. Greco, J. C. O'Donnell, L. A. Spruce, R. Xiao, W. Guo, M. Putt, S. Seeholzer, H. Ischiropoulos, M. B. Robinson, Co-compartmentalization of the astroglial glutamate transporter, GLT-1, with glycolytic enzymes and mitochondria. *J. Neurosci.* **31**, 18275–18288 (2011).
75. J. G. Jackson, J. C. O'Donnell, H. Takano, D. A. Coulter, M. B. Robinson, Neuronal activity and glutamate uptake decrease mitochondrial mobility in astrocytes and position mitochondria near glutamate transporters. *J. Neurosci.* **34**, 1613–1624 (2014).
76. B. S. Whitelaw, M. B. Robinson, Inhibitors of glutamate dehydrogenase block sodium-dependent glutamate uptake in rat brain membranes. *Front. Endocrinol.* **4**, 123 (2013).
77. S. Feng, M. Ye, H. Zhou, X. Jiang, X. Jiang, H. Zou, B. Gong, Immobilized zirconium ion affinity chromatography for specific enrichment of phosphopeptides in phosphoproteome analysis. *Mol. Cell. Proteomics* **6**, 1656–1665 (2007).
78. J. Villén, S. P. Gygi, The SCX/IMAC enrichment approach for global phosphorylation analysis by mass spectrometry. *Nat. Protoc.* **3**, 1630–1638 (2008).
79. S. D. Keene, T. M. Greco, I. Parastatidis, S.-H. Lee, E. G. Hughes, R. J. Balice-Gordon, D. W. Speicher, H. Ischiropoulos, Mass spectrometric and computational analysis of cytokine-induced alterations in the astrocyte secretome. *Proteomics* **9**, 768–782 (2009).
80. A. Boissonnet, T. Hévor, J.-F. Cloix, Phenotypic differences between fast and slow methionine sulfoximine-inbred mice: Seizures, anxiety, and glutamine synthetase. *Epilepsy Res.* **98**, 25–34 (2012).
81. N. Kuo, M. Michalik, M. Erecińska, Inhibition of glutamate dehydrogenase in brain mitochondria and synaptosomes by Mg^{2+} and polyamines: A possible cause for its low in vivo activity. *J. Neurochem.* **63**, 751–757 (1994).
82. A. Akabayashi, T. Kato, One-step and two-step fluorometric assay methods for general aminotransferases using glutamate dehydrogenase. *Anal. Biochem.* **182**, 129–135 (1989).
83. M. Munir, D. M. Correale, M. B. Robinson, Substrate-induced up-regulation of Na^+-dependent glutamate transport activity. *Neurochem. Int.* **37**, 147–162 (2000).
84. A. L. Sheldon, M. I. González, M. B. Robinson, A carboxyl-terminal determinant of the neuronal glutamate transporter, EAAC1, is required for platelet-derived growth factor-dependent trafficking. *J. Biol. Chem.* **281**, 4876–4886 (2006).

Acknowledgments: We thank S. Seeholzer and L. Spruce at the Protein and Proteomics Core of the Children's Hospital of Philadelphia Research Institute for assistance with MS/MS sample analysis. HPLC and ^{15}N isotopomer enrichment analyses were performed in the Metabolomic Core Facility, Children's Hospital of Philadelphia. **Funding:** This work was supported by National Institute on Aging (NIA) grant R01-AG13966, National Heart, Lung, and Blood Institute (NHLBI) grant R01-HL054926, and National Institute of Environmental Health Sciences (NIEHS) Center of Excellence in Environmental Toxicology grant P30-ES013508. K.R. was supported by NIA training grant T32-AG000255. O.H. and I.N. were supported by National Institute of Diabetes and Digestive and Kidney Diseases (NIDDK) grant DK-053761. M.Y., I.N., and M.B.R. were supported by National Institute of Child Health and Human Development (NICHD) Intellectual and Developmental Disabilities Research Center (IDDRC) grant P30-HD026979. J.G.J. was partially supported by National Institute of Neurological Disorders and Stroke (NINDS) training grant T32-NS007413. E.N.G., J.G.J., and M.B.R. were supported by NINDS grant R01-NS077773. H.I. is the Gisela and Dennis Alter Research Professor of Pediatrics. **Author contributions:** K.R., P.T.D., and H.I. designed experiments, analyzed data, and wrote the manuscript. K.R. and P.-T.D. performed experiments and analyzed data. P.E. analyzed proteomic data for GO analyses. E.N.K., J.G.J., and M.B.R. helped design experiments and analyze results for GLT1 studies. O.H., Y.D., Ilana Nissim, M.Y., and Itzhak Nissim helped design experiments and analyze results for stable isotopic labeling studies. K.A.S. performed molecular modeling studies and analyzed results. **Competing interests:** The authors declare that they have no competing interests. **Data and materials availability:** The MS data are available at www.research.chop.edu/tools/msms/aaa4312_Raju_Spectra.pdf.

Submitted 4 December 2014
Accepted 18 June 2015
Final Publication 7 July 2015
10.1126/scisignal.aaa4312
Citation: K. Raju, P.-T. Doulias, P. Evans, E. N. Krizman, J. G. Jackson, O. Horyn, Y. Daikhin, I. Nissim, M. Yudkoff, I. Nissim, K. A. Sharp, M. B. Robinson, H. Ischiropoulos, Regulation of brain glutamate metabolism by nitric oxide and S-nitrosylation. *Sci. Signal.* **8**, ra68 (2015).

Science Signaling

Regulation of brain glutamate metabolism by nitric oxide and S-nitrosylation

Karthik Raju, Paschalis-Thomas Doulias, Perry Evans, Elizabeth N. Krizman, Joshua G. Jackson, Oksana Horyn, Yevgeny Daikhin, Ilana Nissim, Marc Yudkoff, Itzhak Nissim, Kim A. Sharp, Michael B. Robinson and Harry Ischiropoulos

Sci. Signal. **8** (384), ra68.
DOI: 10.1126/scisignal.aaa4312

Regulating neuronal glutamate status

The gasotransmitter nitric oxide (NO) is generated by nitric oxide synthase (NOS) and can affect protein function by modifying cysteine residues in a process called S-nitrosylation. Mice lacking the neuronal NOS (nNOS) isoform have a phenotype that could be explained by decreased availability of glutamate, an amino acid that is also an excitatory neurotransmitter. Glutamate is derived from and can be converted to glutamine, and oxidation of glutamate feeds into the energy-providing TCA (tricarboxylic acid) cycle. Raju *et al*. found that mice lacking nNOS showed decreased S-nitrosylation of proteins involved in glutamate metabolism and uptake. In extracts from these mice, conversion of glutamate to glutamine was decreased, oxidation of glutamate was decreased, and glutamate uptake was increased.